ADVANCED MATERIALS INTERFACES
www.advmatinterfaces.de

Nano-Twisted Double Helix Carbon Debris Improves the Wear Resistance of Ultra-Thick Diamond-Like Carbon Coatings

Xudong Sui, Xinyu Wang, Shuaituo Zhang, Mingming Yan, Wensheng Li, Junying Hao,* and Weimin Liu*

Thick diamond-like carbon (DLC) coatings with different silicon (Si) transition layer thickness are deposited by hollow cathode plasma immersion coating technology. The results show that the internal stress of the coating can be tuned by changing the deposition time of Si transition layer, thereby obtaining good adhesion strength. Friction and wear results show that all coatings have good tribological properties. The coating with 8 min Si transition layer (Si-8) demonstrates the lowest friction coefficient ($\mu \approx 0.03$), even achieves ultralow friction ($\mu \approx 0.008$) for a short time. However, the wear rate of Si-8 coating is found to be the largest (2.1×10^{-16} m^3 (N m)$^{-1}$. The low friction coefficient of Si-8 coating is related to its high degree of graphitization, complete transfer film and fine wear debris. In contrast, the Si-16 coating has the lowest wear rate of about 5.6×10^{-17} m^3 (N m)$^{-1}$ with a relatively high friction coefficient ($\mu \approx 0.1$). This is due to its high hardness and the formation of a nano-twisted double helix carbon debris during the friction process. This nano-twisted double helix structure can consume additional plastic deformation energy, while reducing the interface contact area and increasing the interface bearing capacity, thereby improving the wear resistance of the thick DLC coating.

1. Introduction

Diamond-like carbon (DLC) coatings have attracted great interest in friction lubrication application for its high hardness, low friction, excellent chemical inertness and good biocompatibility.[1–3] They are widely used in automotive energy saving, biological implants, aerospace and other industries.[3–5] In the past few decades, many studies have been conducted to study the friction and lubrication mechanism of DLC coatings.[6–8] For example, Fontaine et al.[8] pointed out that the low friction of the a-C:H film is always attributed to the formation of a smooth transfer film, and controlling the rheology of the transfer film and the composition of the sliding surface can achieve super-low friction of the DLC coating. Donnet and Grill systematically studied the tribological performance and mechanisms of DLC and doped DLC coatings.[9,10] Berman et al.[11] demonstrated a nanoscroll structure formed when graphene is utilized combined with nanodiamond particles and DLC, which achieves superlubricity on an engineering scale. However, due to the problem of excessive stress inside the coating, the above studies have mostly focused on DLC coatings having a thickness of less than 5 µm. Research on the friction and lubrication behavior of the ultra-thick DLC coating (usually refers to coatings larger than 10 µm) is rarely reported, which seriously hindered the advanced tribological applications of these materials.

It is well known that under the premise of good bonding strength, increasing the thickness of the DLC coating can improve the wear resistance, prolong the service life of components, and thus reduce the product cost. Recently, many efforts have been devoted to produce high quality ultra-thick DLC coatings, such as developing new technologies, designing interface, applying plasma treatments and so on.[12–14] For example, Wang et al.[12] prepared an ultra-thick DLC coating with a thickness of about 50 µm by hollow cathode plasma-enhanced chemical vapor deposition method. The deposited ultra-thick DLC coating has good tribological performance with a friction coefficient less than 0.2 in air condition. Figueroa et al.[13] designed a Silicon (Si) containing interlayer and achieved a high adhesion force of the DLC coating on ferrous alloys by applying high-bias voltage (800 V) and low temperature (150 °C). Oka and Yatsuzuka used a carbon ion implantation treatment after sputter cleaning to achieve the adhesion force of DLC coating of more than 70 MPa.[14]

The purpose of this work is to obtain well-bonded ultra-thick DLC coatings via hollow cathode plasma immersion coating

Prof. X. Sui, X. Wang, S. Zhang, M. Yan, Prof. J. Hao, Prof. W. Liu
State Key Laboratory of Solid Lubrication
Lanzhou Institute of Chemical Physics
Chinese Academy of Sciences
Lanzhou 730000, China
E-mail: suixudong@licp.cas.cn; jyhao@licp.cas.cn
Prof. X. Sui, X. Wang, S. Zhang, M. Yan, Prof. J. Hao
Center of Materials Science and Optoelectronics Engineering
University of Chinese Academy of Sciences
Beijing 100049, China
Prof. X. Sui, S. Zhang, Prof. J. Hao
Qingdao Center of Resource Chemistry and New Materials
Qingdao 266000, China
Prof. W. Li
State Key Laboratory of Advanced Processing
and Recycling of Nonferrous Metals
Lanzhou University of Technology
Lanzhou 730050, China
The ORCID identification number(s) for the author(s) of this article can be found under https://doi.org/10.1002/admi.202000857.

DOI: 10.1002/admi.202000857

technology, by properly designing the thickness of Si transition layer. The relationship between the structural, mechanical and tribological properties of these ultra-thick DLC coatings has been systematically investigated. Finally, we shall analyze the transfer layer behavior and wear mechanism of the coatings.

2. Experimental Section

2.1. Sample Preparation

The Si/Si-DLC/DLC thick coatings were deposited using three gas sources of acetylene (C_2H_2), argon (Ar) and silane (2% SiH_4 + Ar) in a small (56 × 560 mm) tubular vacuum chamber (**Figure 1**a). Two types of substrate materials were used for depositing the coating. Silicon wafers were mainly used for structural characterization and AISI 440C steel substrates were mainly used for mechanical and tribological characterization. During the deposition process, a hollow cathode discharge effect was created inside the vacuum chamber by applying a pulsed negative bias on the tubular vacuum chamber. The samples were placed inside the chamber for fast and efficient deposition of carbon-based coatings. More details on the principle of this coating method can be found in our previously published literature.[15] Before deposition, the substrate was first cleaned in a hydrogen plasma for 15 min with a bias of 350 V. Subsequently, in order to adjust the adhesion strength and the internal stress, Si transition layers with different thicknesses were first deposited by controlling the deposition time to 0, 8, 16 and 32 minutes, respectively, under a silane flow of 400 sccm. After this layer, a Si-doped DLC intermediate layer was obtained by introducing a mixture of acetylene and silane in a vacuum chamber to further reduce stress. The flow rate of acetylene was controlled to gradually increase from 0 to 150 sccm in 1 hour, while the flow rate of silane gradually decreased from 400 to 0 sccm. Finally, a pure DLC top layer is deposited on the surface in acetylene and argon atmosphere, producing Si/Si-DLC/DLC multilayer coatings. The total deposition pressure was 70 mTorr and the applied power was maintained at 275 W during the deposition process. For the convenience of the discussion, Si-0, Si-8, Si-16 and Si-32 were used to represent the as-deposited coating samples with different thickness of the Si transition layer. It is evident from Figure 1b that the coating deposited herein was an ultra-thick DLC coating (≈20 µm) compared to the conventional DLC coatings.

2.2. Coating Characterization

The morphology and thickness of the coating was examined by field emission scanning electron microscopy (FE-SEM, JSM-6700F). The composition was analyzed by energy dispersive spectrometer (EDS). Raman signals of the coatings were detected by a spectrometer (Horiba, LabRam HR Evolution) at an excitation wavelength of 532 nm. A focused ion beam (FIB, Gatan 695) lift-out technique was used to prepare thin sections of the selected wear debris and then analyzed by high resolution transmission electron microscope (HRTEM, FEI Talos F200).

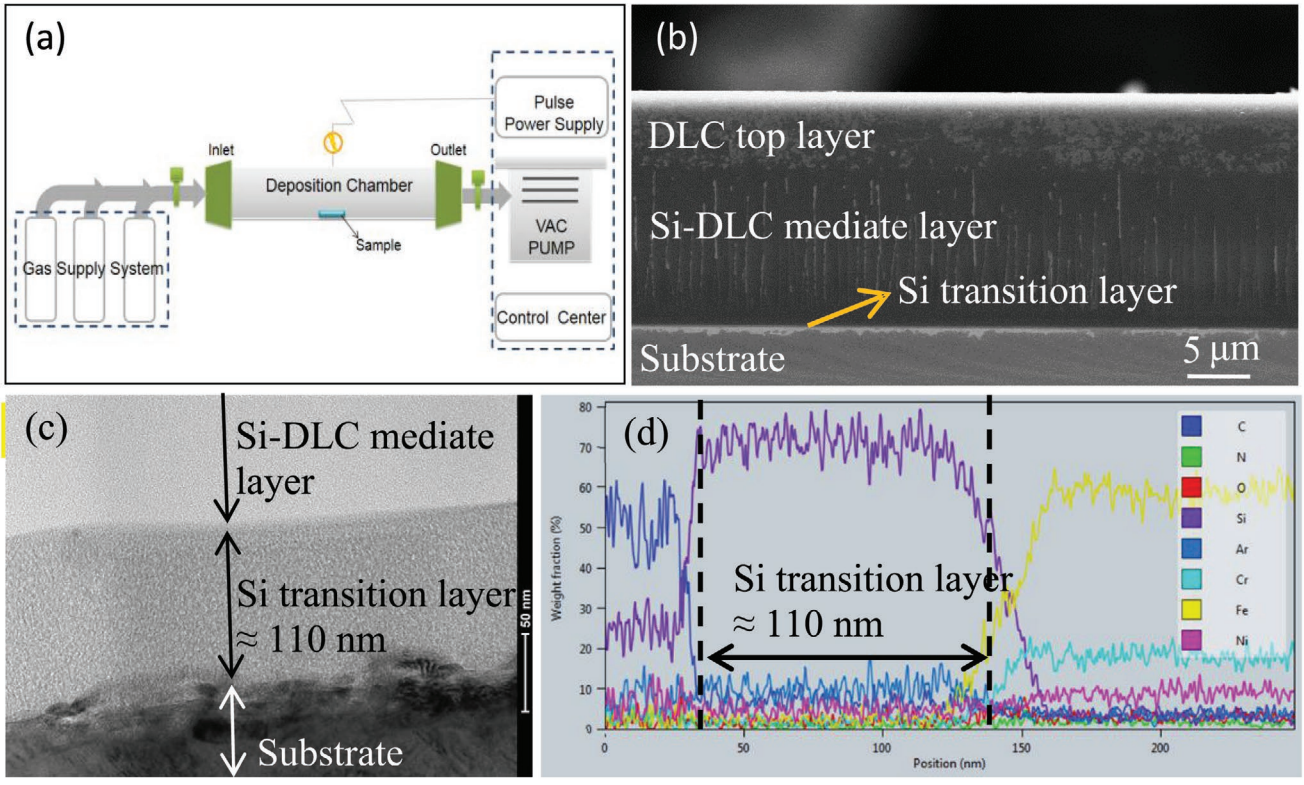

Figure 1. a) Schematic diagram of a hollow cathode plasma immersion coating system. b) The SEM cross-section image. c) TEM cross-section of the Si-8 sample and d) the corresponding EDS line scan result.

The adhesion strength between the coating and the substrate was characterized using a multifunctional surface property tester (MFT-4000, Lanzhou Huahui). A nano-indenter (Agilent, Nano Indenter XP) with a Berkovich diamond tip was used to characterize the hardness and elastic modulus of the coatings. In order to minimize the substrate's influence, the indentation depth was controlled at about 200 nm, and each sample was tested five times. The elastic recovery rate (W_e) of the coating was given by the equation[16]:

$$W_e = (d_{\max} - d_{\text{res}})/d_{\max} \times 100\% \quad (1)$$

where $d_{\max}$ and d_{res} are the maximum and residual displacement, respectively. The internal stress of the coating was calculated by the Stoney's equation[17]:

$$\sigma = -\frac{E_S h_s^2}{6(1-v_s)h_c}\left(\frac{1}{R_a}-\frac{1}{R_b}\right) \quad (2)$$

where E_s and v_s are elastic modulus and poisson's ratio of the substrate, h_s and h_c are the thickness of the substrate and the coating, R_a and R_b are the spherical radii of curvature detected by MicroXAM-3D surface profile after and before deposition, respectively. The tribological properties were investigated by a ball-on-disk CSM tribometer using AISI 440C ball (φ 6 mm) as friction pair in laboratory air of 10% relative humidity. The friction tests were carried out at a sliding speed of 10 cm s^{-1} under a normal load of 3 N. The calculated Hertz contact stress during the tests is about 660 MPa. The total sliding distance was 1500 m, and the profile morphology of the wear scars was measured by an optical profile every 500 m. The wear rate k was calculated by the following equation[18]:

$$k = V/SN \quad (3)$$

where V is the wear volume; S is the total sliding distance; N is the normal load.

3. Results and Discussion

3.1. Structure and Mechanical Properties

Figure 1b shows the cross-section SEM image of the Si-8 sample. It can be found that the coating is divided into three layers: (a) Si transition layer, (b) Si-DLC mediate layer and (c) DLC top layer. Due to the transitional design between layers, it is not easy to observe obvious delamination at the resolution of the scanning electron microscope, especially for the Si transition layer with a thickness of several hundred nanometers. In order to verify the existence of the Si transition layer, a transmission electron microscope (TEM) cross-section sample of Si-8 coating is prepared using FIB technology (Figure 1c). It can be clearly observed from the TEM image that the Si transition layer has a thickness of about 110 nm. The composition and thickness of this Si transition layer are also confirmed from the results of EDS line scanning under TEM as shown in Figure 1d. In this work, by controlling the deposition time of Si transition layer to 0, 8, 16 and 32 minutes, respectively, we can easily obtain a series of coating samples with different Si transition layer thickness. Due to time and cost constraints, we did not perform FIB and TEM observations on the thickness of the Si transition layer for each sample. However, there is a consensus in the vacuum coating industry, that is, when other parameters remain unchanged, the longer the deposition time, the thicker the film thickness. Therefore, we can adjust the thickness of the Si transition layer by controlling the deposition time.

The Raman analysis results were shown in **Figure 2**a. The Raman spectra of all coatings are very similar, exhibiting two Gaussian fitted peaks (D peak and G peak). The D peak is derived from the breathing mode of sp^2 carbon atoms in rings, and G peak is attributed to the stretching vibration symmetry of a pair of sp^2 atoms in aromatic rings or chains.[19] By calculating the intensity ratio of the D peak to the G peak, we can obtain the I_D/I_G value of the coatings as shown in the inset picture in Figure 2a. This is an important structural indicator for DLC coating.[19–21] Generally, a higher I_D/I_G value means more graphitization of the coating.[22–26] It can be found that with the increase of the deposition time of the Si transition layer, the I_D/I_G value of the coating peaks at 0.98 (Si-8 sample), and then gradually decreases to 0.90 (Si-32 sample). This may be the result of changes in substrate temperature during the deposition process. The increase in the thickness of Si layer may result in a higher discharge voltage during the subsequent coating process. When the deposition power is kept constant, the thicker the Si layer, the smaller the current inside the pipe, which means that the plasma density decreases. The decrease in plasma density will cause the temperature inside the pipe cavity to decrease, which will affect the structure of the top carbon film. Figure 2b shows the load-displacement curves of the coatings during the nanoindentation test. It is worth noting that all of the coatings exhibit satisfactory elastic recovery of about 70% after unloading, suggesting that the reversible deformation is predominant during indentation test (Figure 2c). Excellent elasticity can improve the anti-bearing capacity of the ultra-thick DLC coating and improve the wear resistance.[18] Figure 2d gives the hardness results of the coatings. It can be found that the hardness of all samples exceed 10 GPa. The hardness of the Si-8 sample is lower than that of other samples, which is consistent with the Raman results.

Figure 3a presents the residual stress results of the coating. As can be found that the residual stress of all coatings is negative, which means that there is compressive stress inside the prepared coatings. With the increment of the Si transition layer increasing, the absolute value of the residual stress of the coating decreases first and then increases, and the minimum value is obtained when the deposition time of the Si transition layer is 8 min. This also explains the lowest hardness of the Si-8 sample. In general, residual stress has a significant effect on the adhesion strength of the coating, which is a major problem for the conventional method in preparing a thick DLC coating (>5 μm).[12,27] In our work, except for a slightly smaller critical load of the Si-32 sample, the other coatings own a critical load of more than 35 N, showing good adhesion strength. It can be seen from Figures 3c–f that no significant peeling of the coating occurred until the critical load was reached. In short,

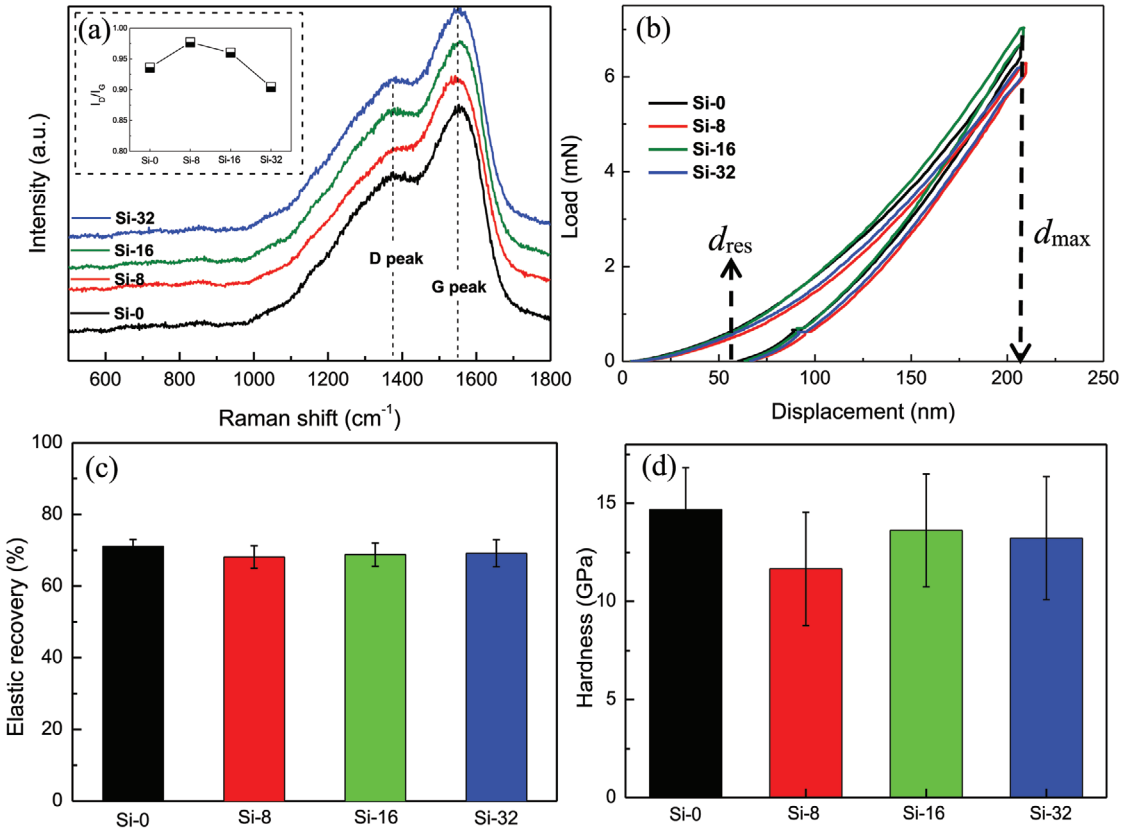

Figure 2. a) Raman spectroscopy and b) load-displacement curves of the prepared coatings, c) the results of elastic recovery and d) hardness of the coatings during the nanoindentation test.

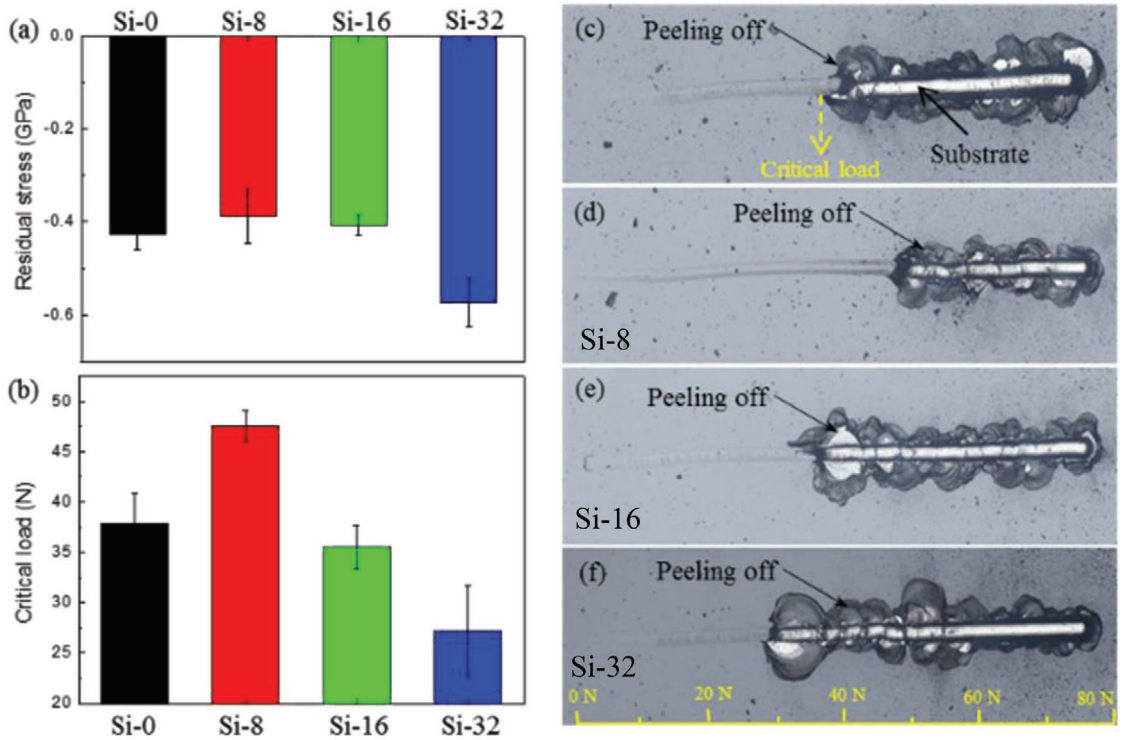

Figure 3. a) Residual stress and b) critical load of the as-deposited coatings, c–f) the corresponding scratch morphology of the coatings.

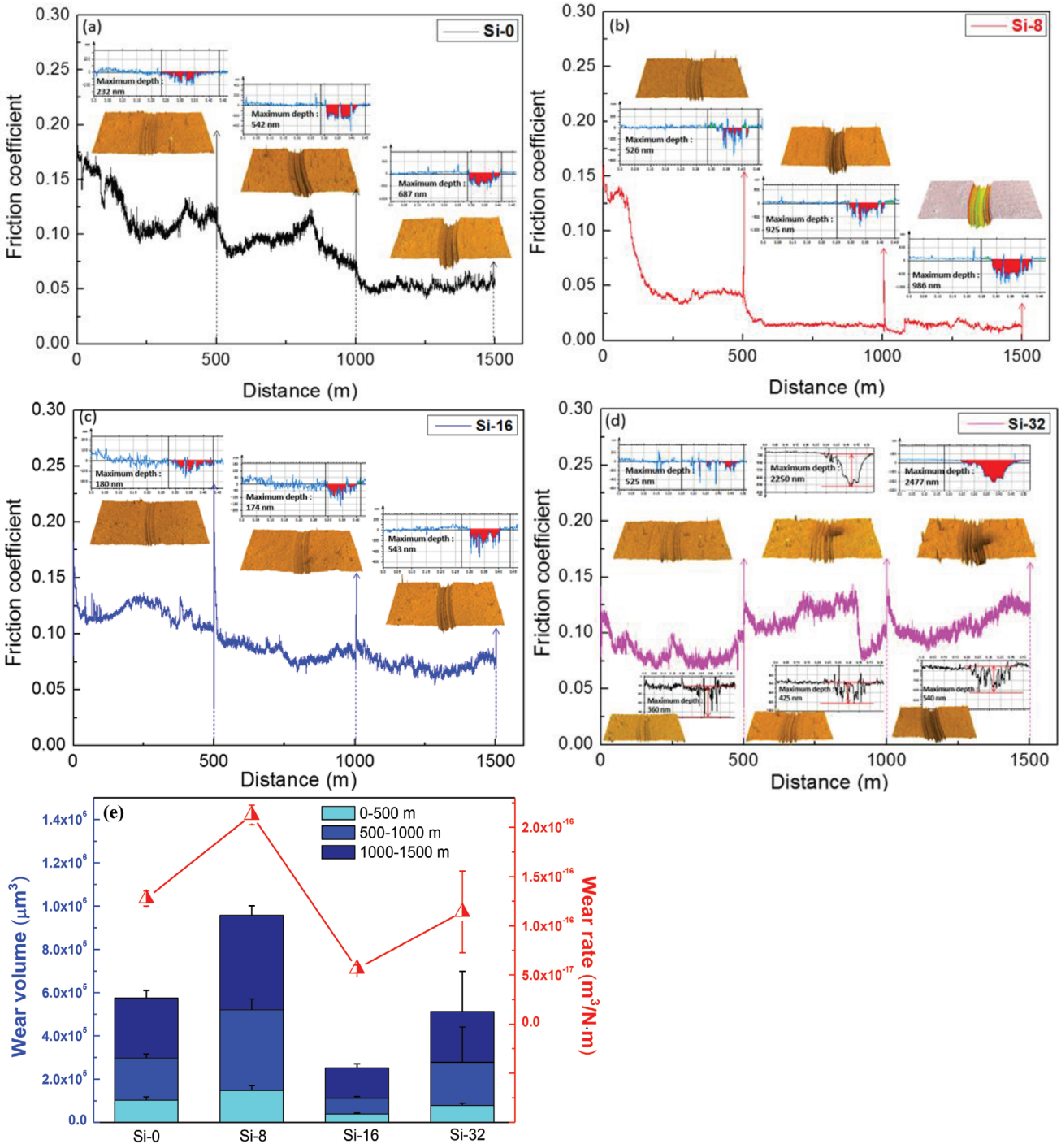

Figure 4. a–d) Friction coefficient, wear morphology and e) wear rate of the as-deposited coatings.

the adhesion and residual stress of the coating are negatively correlated in this work.

3.2. Friction and Wear Performance

Experiments under dry friction conditions (cf. **Figure 4**a–d) revealed all deposited ultra-thick DLC coatings have excellent frictional performance. In the initial stage of friction, since no friction transfer film is formed, the coefficient of friction of the coating is relatively high, between about 0.1 and 0.18. As the friction progresses, a transfer layer with good lubricating properties is formed at the interface between the coating and ball under the effect of stress and frictional heat. Then the friction coefficient of the coating is lowered. The average coefficients of friction of all coatings are less than about 0.1.

It is worth noting that the Si-8 coatings own the lowest friction coefficient, which is close to ultralow friction (0.01). This may be related to the higher degree of graphitization of the Si-8 coating. As can be seen from the insets in Figure 4, the 3D profile measurement of the wear scar is conducted every 500 m to evaluate the wear resistance of the coating. It can be observed that the wear scars of the Si-0, Si-8 and Si-16 coatings show clear edges and shallow depths. In contrast, the Si-32 coating exhibits two types of wear scar morphology: one is a uniform wear scar morphology as shown in the bottom 3D images of Figure 4d, and the other is the local coating peeling as shown in the top 3D images of Figure 4d. The abnormal wear occurring in the Si-32 coating is related to its high internal stress and poor adhesion strength. Figure 4e presents the wear rate of the prepared coatings. It is worth noting that the wear rate of the Si-8 coating (Figure 4e) was found to be the largest (2.1×10^{-16} m^3 $(N\ m)^{-1}$, while the Si-16 sample had the lowest wear rate of about 5.6×10^{-17} m^3 $(N\ m)^{-1}$. The friction coefficient and wear rate of the coating do not show the usual positive correlation, which is a very interesting phenomenon. Generally, the wear resistance of the coating is most closely related to the adhesion strength and hardness. Since the thickness of the coating prepared in this work reached more than ten microns, the wear only occurred a few hundred nanometers to three microns below the surface during the friction test, and no obvious flaking occurred. Thus, it can be considered that the wear resistance of the coating in this work is mainly affected by the hardness. As shown in Figure 2d, the Si-8 sample has the lowest hardness, thus showing the highest wear.

3.3. Wear Morphology and Mechanism

To explain the wear mechanism of the thick DLC coatings in this work, we have carefully studied the wear debris on the corresponding coating surface (**Figures 5**a–d) and friction pair (Figures 5e–l). It can be found from Figures 5a–d that all thick DLC coatings exhibit a scratched track surface, meaning that groove wear has occurred. In addition, the Si-32 coating also exhibits significant peeling wear, which is consistent with the results observed by the 3D profilometer. Figures 5e–h give the SEM images of the corresponding friction ball. It can be observed that the wear scar of the Si-8 coating is the smallest and the formed lubrication transfer film is the most complete and smooth. This also explains why the Si-8 coating has the lowest friction coefficient. As the deposition time of Si transition layer increases, the area of the wear scars and the number of wear debris gradually increase. And the lubrication transfer film on the Si-32 coating becomes very discontinuous, and the surface also shows more scratches. This is also consistent with the friction coefficient results. Figures 5i–l show the enlarged SEM images of the corresponding wear debris. It is worth noting that the Si-0, Si-8, and Si-32 coatings only generated a kind of flake-like wear debris, and the size of the wear debris of Si-8 coating is smallest. However, it is evident from Figure 5k that the Si-16 sample has

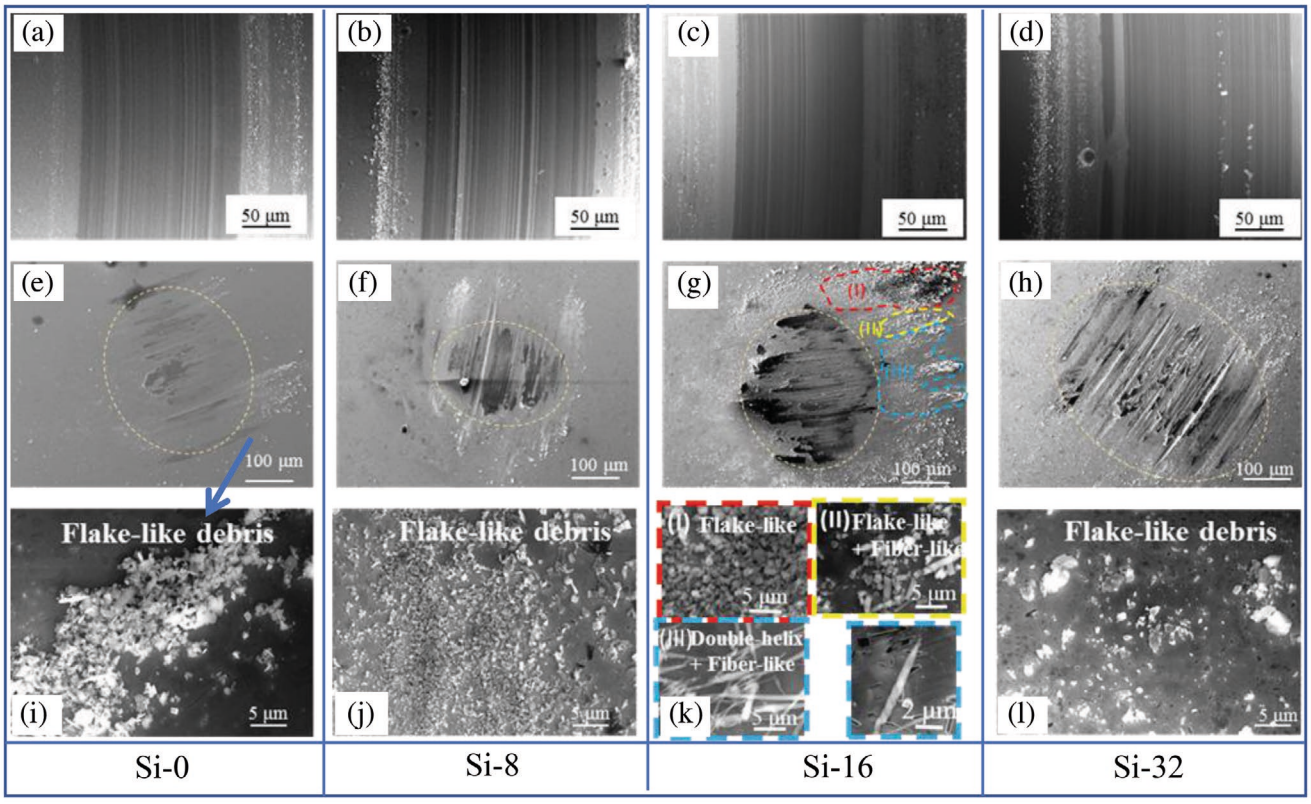

Figure 5. a–d) SEM images of the wear tracks on the coating surface and e–h) the friction pair. i–l) The wear debris on the corresponding friction pair.

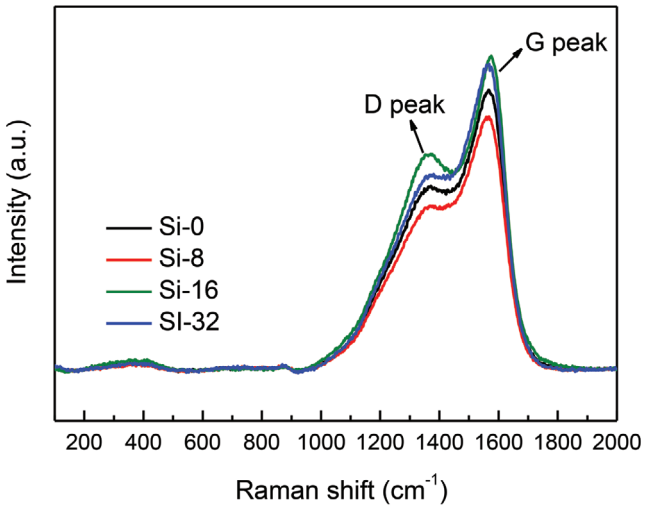

Figure 6. Raman spectroscopy of wear tracks of the deposited coatings.

three type of wear debris: (1) Flake-like debris, mainly appearing at the edges on both sides of the sliding direction; (2) Nano-twisted double helix debris, mainly distributed on the back of the wear scar in the sliding direction; (3) Fiber-like debris, distributed in the transition zone among the above two types of wear debris. In the Supporting Information, we can see clearer images of this unique wear debris and EDS detection found that the main component of this nano double helix structure is carbon (Figure S1, Supporting Information). **Figure 6** gives the Raman results of the wear track of the deposited coatings. As can be seen from the picture, the D peak of the Si-16 sample becomes sharper after friction, which means that the ordered carbon structure in the wear track increases. In contrast, the D peak of wear track of the Si-8 sample is board and not obvious. This may be due to the fact that the friction coefficient of the Si-16 sample is much higher than that of the Si-8 sample, which generates more friction heat, resulting in an increased ordering of the carbon film in the contact area.

To further determine the structure of this unique wear debris, it was taken out from the surface of the friction pair using an FIB technique, as shown in **Figure 7**. First, we found these nano-twisted double helix wear debris under an electron microscope (Figure 7a). Then we used EDS mapping scan to confirm that the elements were correct (Figure 7b). Finally, a Pt protective layer was deposited and a TEM sample, processed using FIB. As shown in Figure 7c, the bright white strip in the middle is the wear debris, and the top and bottom are the Pt protective layer and the 440C steel ball, respectively. The obtained HRTEM micrograph of the cross-section of the coating is shown in Figure 7d. It is easy to observe a highly crosslinking network carbon nanostructure. A close view of the morphology shows some parallel-curved basal planes (Figure 7f) dispersing in an amorphous carbon matrix. This is similar to the presence of a fullerene-like structure in the carbonaceous coating reported in the literature.[28] The fast fourier transform (FFT) diffraction patterns of the wear debris show two diffuse rings with lattice spacing of 2.38 and 2.74 Å, respectively. These match well with the spacing of fullerene C60 (d_{531} = 2.40 Å and

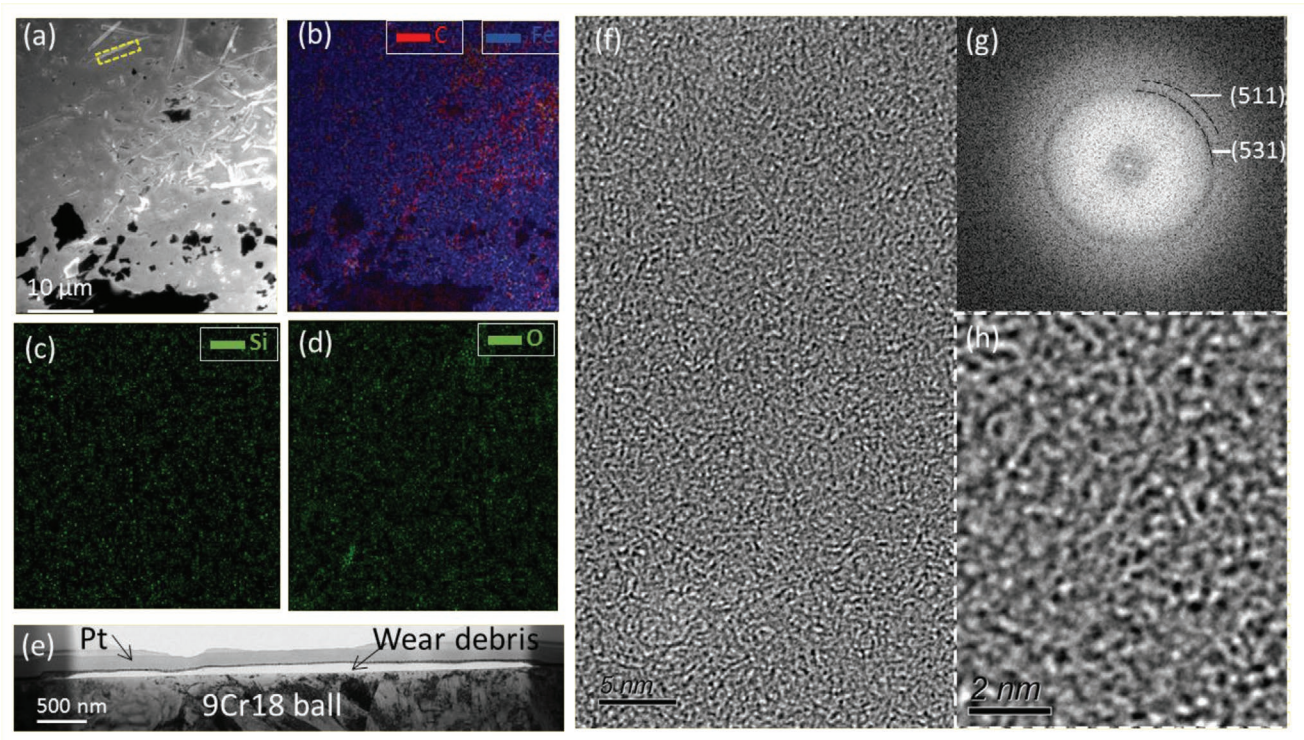

Figure 7. FESEM image a) and EDS mapping result b–d) of the wear debris of the Si-16 sample.e) The corresponding TEM debris sample made by FIB lift-out method. f) The corresponding HRTEM images of the wear debris. g) The corresponding FFT image. (h) The magnified view of the HRTEM image of the wear debris.

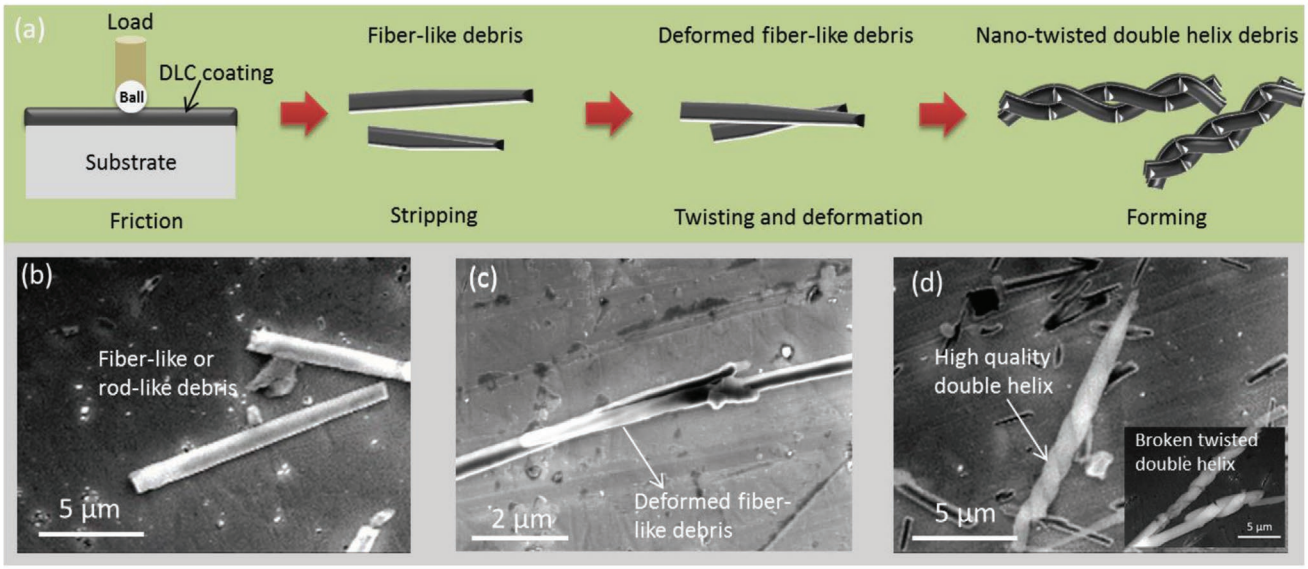

Figure 8. Schematic diagram of the formation mechanism of a) nano-twisted double helix wear debris and b–d) typical SEM images of the wear debris of the Si-16 coating .

d_{511} = 2.73 Å). In the Supporting Information, the Raman spectroscopy also exhibits the existence of fullerene structure in the coating (Figure S2, Supporting Information).[29] Therefore, this nano-twisted double helix wear debris own a composite nanostructure comprising a fullerene-like structure and an amorphous carbon skeleton.

Previous studies have proved that the curved graphene sheets in the fullerene-like structure can prevent relative sliding and achieve excellent elastic recovery by local bending.[30] Similarly, Hauert reported a fiber-like wear debris in his previous review article. The Auger spectrum showed that this fiber-like debris is contained only in carbon and was mechanically closer to the plastic and polymer-like.[31,32] So, we can speculate that the formation mechanism of the nano-twisted double helix debris in this paper is as shown in **Figure 8**. Firstly, the fiber or rod-like debris (Figure 8b) are peeled off from the coating surface by friction; secondly, these fiber-like debris are repeatedly rubbed along the sliding direction and twisted together to form a double helix structure by plastic deformation. The nano-twisted double helix debris in the Figure 8d may be formed by twisting two fiber-like debris in Figures 8b,c. Honestly, there are many possible factors that affect the formation of this nano-twisted double helix structure, like internal stress, hardness, elasticity, etc. The formation mechanism of this special nano-twisted double helix structure still needs to be studied further. However, we can be sure that the coating should have good elasticity and toughness to form a high quality double helix structure without breakage. Since the plastic deformation occurs during the formation of the nano-twisted double helix debris, it will consume additional plastic deformation energy.[31] At the same time, due to the presence of the nano-twisted double helix debris, the contact area between the coating and the friction pair is reduced. Moreover, the formed robust but yet double helix structure can endow the interface with a higher anti-bearing ability. As a result, the prepared thick DLC coating obtains excellent wear resistance.

4. Conclusion

In summary, this study has discussed a series of ultra-thick DLC coatings which own a highly elastic ultra-thick nanocomposite structure. Friction and wear results show that all the coatings have good tribological properties. The coatings prepared under the condition that the Si transition layer is deposited for 8 minutes have the lowest friction coefficient, which is close to ultralow friction (0.01). However, this coating has the highest wear rate in the series prepared. In contrast, the coating prepared with 16 minutes Si transition layer owns the lowest wear rate, although its friction coefficient is relatively high. The above results may be due to the combination of the coating characteristics and the effect of the wear debris during the friction process. The unique nano-twisted double helix carbon debris was found during rubbing process of the ultra-thick DLC coating with 16 minutes Si transition layer. This original debris structure may consume additional plastic deformation energy, leading to an increase in the friction coefficient. But at the same time, the interface contact area is decreased and the interface bearing capacity is increased, thereby improving the wear resistance of the coating.

Supporting Information

Supporting Information is available from the Wiley Online Library or from the author.

Acknowledgements

The authors gratefully acknowledge the financial support of the National Key R&D Plan of China (No. 2018YFB0703803), National Natural Science Foundation of China (51835012, 51805515), the program of "Science & Technology International Cooperation Demonstrative Base of Metal Surface Engineering along the Silk Road (2017D01003)," and CAS "Light of West China".

Conflict of Interest

The authors declare no conflict of interest.

Keywords

diamond-like carbon, friction and wear, nano-twisted double helix, wear debris

Received: May 15, 2020
Revised: July 22, 2020
Published online:

[1] J. Robertson, *Mater. Sci. Eng., R.* **2002**, *37*, 129.
[2] S. W. Liu, C. H. Zhang, E. Osman, X. C. Chen, T. B. Ma, Y. Z. Hu, J. B. Luo, E. Ali, *Sci. China: Technol. Sci.* **2016**, *59*, 1795.
[3] X. Q. Fan, Q. J. Xue, L. P. Wang, *Friction* **2015**, *3*, 191.
[4] N. Dolatabadi, M. Forder, N. Morris, R. Rahmani, H. Rahnejat, S. Howell-Smith, *Appl. Energy* **2020**, *259*, 114.
[5] D. Nandakumar, A. Bendavid, P. J. Martin, K. D. Harris, A. J. Ruys, M. S. Lord, *ACS Appl. Mater. Interfaces* **2016**, *8*, 6802.
[6] N. S. Tambe, B. Bhushan, *Scr. Mater.* **2005**, *52*, 751.
[7] J. Fontaine, J. L. Loubet, T. L. Mogne, A. Grill, *Tribol. Lett.* **2004**, *17*, 709.
[8] J. Fontaine, T. L. Mogne, J. L. Loubet, M. Belin, *Thin. Solid. Films.* **2005**, *482*, 99.
[9] C. Donnet, *Surf. Coat. Technol.* **1998**, *100–101*, 180.
[10] A. Grill, *Wear* **1993**, *168*, 143.
[11] D. Berman, S. A. Deshmukh, S. K. R. S. Sankaranarayanan, A. Erdemir, A. V. Sumant, *Science* **2015**, *348*, 1118.
[12] J. J. Wang, J. B. Pu, G. G. Zhang, L. P. Wang, *ACS Appl. Mater. Interfaces* **2013**, *5*, 5015.
[13] A. E. Crespi, L. M. Leidens, V. Antunes, B. L. Perotti, A. F. Michels, F. Alvarez, C. A. Figueroa, *ACS Appl. Mater. Interfaces* **2019**, *11*, 18024.
[14] Y. Oka, M. Yatsuzuka, *Nucl. Instrum. Methods Phys. Res., Sect. B* **2019**, *449*, 58.
[15] X. Y. Wang, X. D. Sui, S. T. Zhang, M. M. Yan, J. Yang, J. Y. Hao, W. M. Liu, *Surf. Coat. Technol.* **2019**, *375*, 150.
[16] X. Q. Liu, J. Y. Yang, J. Y. Hao, J. Y. Zheng, Q. Y. Gong, W. M. Liu, *Adv. Mater.* **2012**, *24*, 4614.
[17] J. Tamayo, J. J. Ruz, V. Pini, P. Kosaka, M. Calleja, *Nanotechnology* **2012**, *23*, 475702.
[18] X. D. Sui, J. Y. Liu, S. T. Zhang, J. Yang, J. Y. Hao, *Appl. Surf. Sci.* **2018**, *439*, 24.
[19] A. C. Ferrari, J. Robertson, *Phys. Rev. B* **2000**, *61*, 14095.
[20] A. C. Ferrari, J. Robertson, *Phys. Rev. B* **2001**, *64*, 075414.
[21] Y. J. Wang, H. X. Li, L. Ji, F. Zhao, X. H. Liu, Q. H. Kong, Y. X. Wang, W. L. Quan, H. D. Zhou, J. M. Chen, *J. Phys. D:Appl. Phys.* **2010**, *43*, 505401.
[22] S. Yamamoto, A. Kawana, H. Ichimura, C. Masuda, *Surf. Coat. Technol.* **2012**, *210*, 1.
[23] S. M. Chiu, S. C. Lee, C. H. Wang, F. C. Tai, C. W. Chu, D. Gan, *J. Alloys Compd.* **2008**, *449*, 379.
[24] A. C. Ferrari, J. Robertson, *Philos. Trans. R. Soc., A* **2004**, *362*, 2477.
[25] X. R. Shi, T. W. Liskiewicz, B. D. Beake, J. Chen, C. Wang, *Tribol. Int.* **2020**, *149*, 105586.
[26] L. Huang, J. T. Yuan, C. Li, D. B. Hong, *Surf. Coat. Technol.* **2018**, *353*, 163.
[27] X. Li, B. Bhushan, *J. Mater. Res.* **1999**, *14*, 2328.
[28] B. Zhang, Y. Zhou, J. Y. Zhang, Z. Wang, *Surf. Interface Anal.* **2012**, *44*, 162.
[29] Q. Wang, C. B. Wang, Z. Wang, J. Y. Zhang, D. Y. He, *Appl. Phys. Lett.* **2007**, *91*, 141902.
[30] I. Alexandrou, H. J. Scheibe, C. J. Kiely, A. J. Papworth, G. A. J. Amaratunga, B. Schultrich, *Phys. Rev. B.* **1999**, *60*, 10903.
[31] R. Hauert, *Tribol. Int.* **2004**, *37*, 991.
[32] F. Fukui, M. Irie, Y. Utsumi, K. Oda, H. Ohara, *Surf. Coat. Technol.* **2001**, *378*, 146.